Electronic Supplementary Information (ESI)

# Transition Metal Anchored $C_2N$ Monolayers as Efficient Bifunctional Electrocatalysts for Hydrogen and Oxygen Evolution Reactions

Xu Zhang,[a‡] An Chen,[ab‡] Zihe Zhang,[a] Menggai Jiao,[a] Zhen Zhou*[a]

[a] School of Materials Science and Engineering, National Institute for Advanced Materials, Institute of New Energy Material Chemistry, Collaborative Innovation Centre of Chemical Science and Engineering (Tianjin), Computational Centre for Molecular Science, Nankai University, Tianjin 300350, P. R. China

[b] College of Material Science and Engineering, Northeast Forestry University, Harbin 150040, P. R. China

*Corresponding Authors. Email: zhouzhen@nankai.edu.cn (Z.Z.)

Table S1. The binding energy $E_b$ (eV) and atomic charge a.c. (|e|) of anchoring TM atoms at three possible sites. The most stable configurations are highlighted in red typeface. – represents that after the structural optimization, the anchoring TM atoms move to another sites.

| | $E_b$ (i) | $E_b$ (ii) | $E_b$ (iii) | a.c. (i) | a.c. (ii) | a.c. (iii) |
|---|---|---|---|---|---|---|
| Ti | -7.57 | -7.53 | -7.78 | 1.50 | 1.68 | 1.52 |
| Mn | -4.65 | -4.75 | -4.74 | 1.33 | 1.32 | 1.32 |
| Fe | -4.74 | -4.94 | -5.04 | 1.12 | 1.16 | 1.16 |
| Co | -4.32 | -4.95 | – | 0.99 | 0.88 | – |
| Ni | -3.64 | -4.76 | – | 0.80 | 0.79 | – |
| Cu | -3.20 | -3.53 | – | 0.72 | 0.73 | – |
| Mo | -5.09 | -5.77 | -5.79 | 1.40 | 1.30 | 1.30 |
| Ru | – | -5.55 | -5.53 | – | 0.95 | 0.78 |
| Rh | -4.40 | -5.50 | -5.51 | 0.78 | 0.67 | 0.67 |
| Pd | -3.07 | -3.53 | -3.29 | 0.54 | 0.59 | 0.59 |
| Ag | -3.17 | – | – | 0.64 | – | – |
| Ir | -4.35 | -6.15 | -6.23 | 0.69 | 0.66 | 0.66 |
| Pt | -3.39 | -4.45 | -4.53 | 0.52 | 0.66 | 0.70 |
| Au | -2.45 | - | - | 0.47 | - | - |

Table S2. The binding energy $E_b$ (eV) of the second anchoring TM atoms and average atomic charge a.c. (|e|) at two possible sites. The most stable configurations are highlighted in red typeface. – represents that after the structural optimization, the anchoring TM atoms move to another sites.

| | $E_b$ (I) | $E_b$ (II) | a.c. (I) | a.c. (II) |
|---|---|---|---|---|
| Ti | -4.63 | - | 1.13 | - |
| Mn | - | -3.60 | - | 0.83 |
| Fe | -5.04 | -4.37 | 0.75 | 0.77 |
| Co | -4.52 | -4.66 | 0.60 | 0.59 |
| Ni | -5.34 | -4.36 | 0.60 | 0.58 |
| Cu | -3.10 | -2.90 | 0.60 | 0.58 |
| Mo | -6.20 | - | 0.98 | - |
| Ru | - | -6.34 | - | 0.66 |
| Rh | - | -5.13 | - | 0.54 |
| Pd | -3.30 | -2.52 | 0.45 | 0.42 |
| Ag | 0.48 | 0.84 | 0.49 | 0.49 |
| Ir | - | -6.55 | - | 0.57 |
| Pt | -5.89 | -4.32 | 0.44 | 0.39 |
| Au | -0.91 | - | 0.60 | - |

Table S3. The binding energy $E_b$ (eV) of the third anchoring TM atoms.

| | $E_b$ |
|---|---|
| Fe | -3.44 |
| Co | -1.82 |
| Ni | -1.90 |
| Cu | -2.29 |
| Mo | -3.30 |
| Ru | -3.47 |
| Rh | -3.64 |
| Pd | -1.88 |
| Ir | -5.54 |
| Pt | -3.55 |

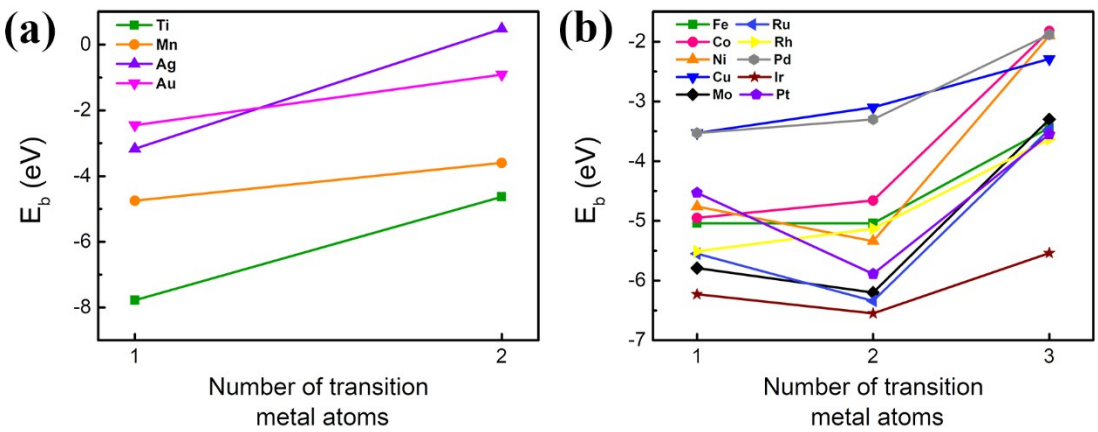


Fig. S1 The binding energies against the number of transition metal atoms.

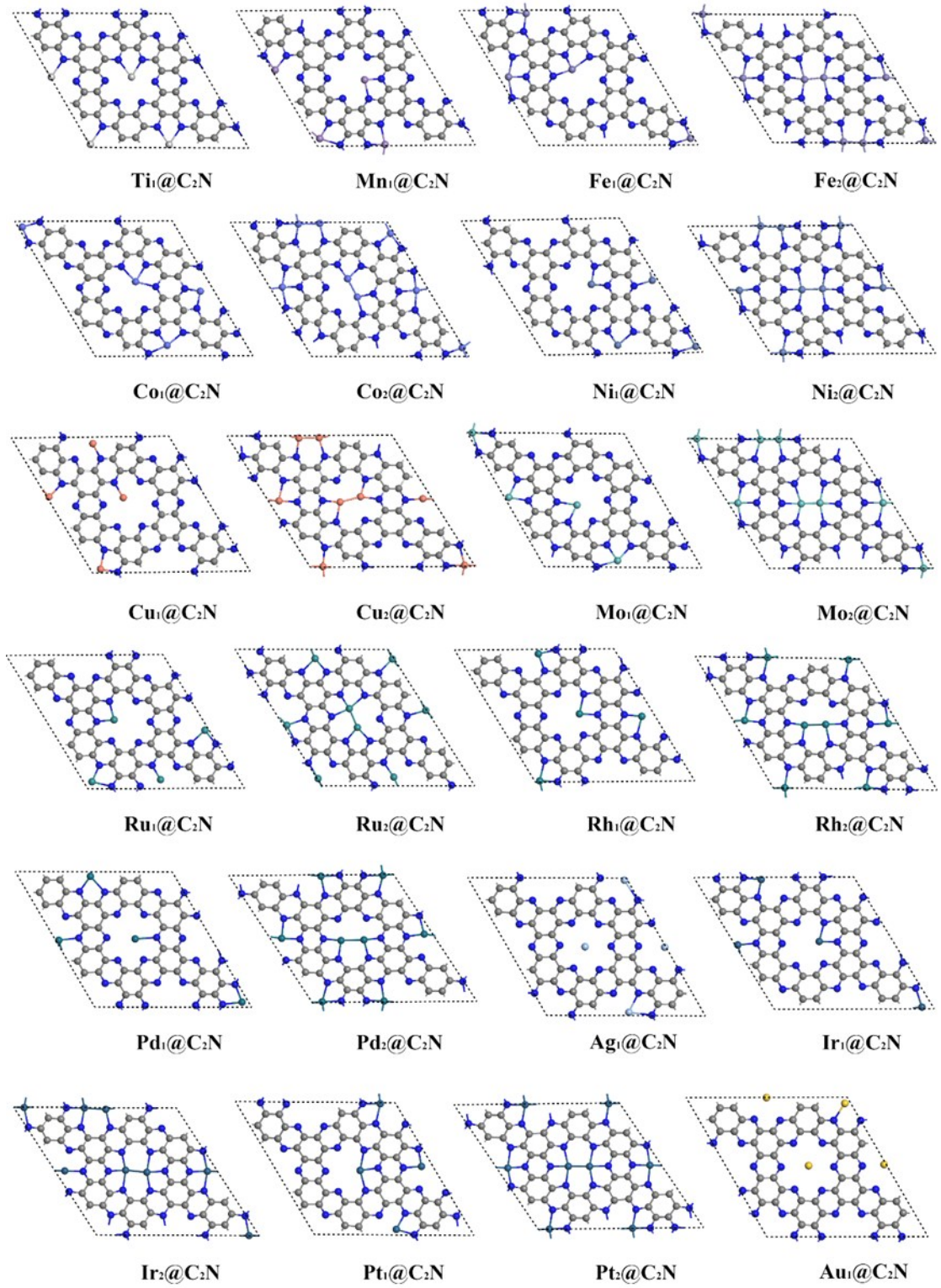


Fig. S2 Snapshots of the equilibrium structure of TMx@C2N at 800 K after 10 ps AIMD simulations.

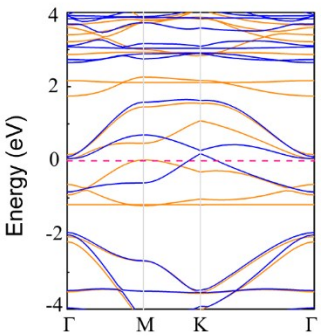


**$Ti_1@C_2N$**

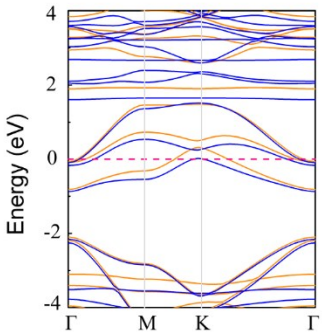


**$Mn_1@C_2N$**

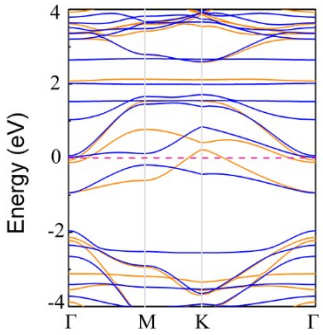


**$Fe_1@C_2N$**

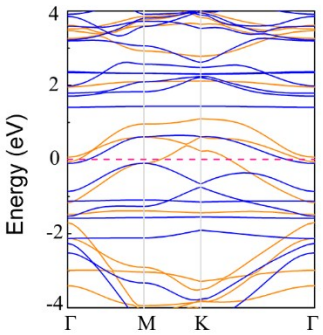


**$Fe_2@C_2N$**

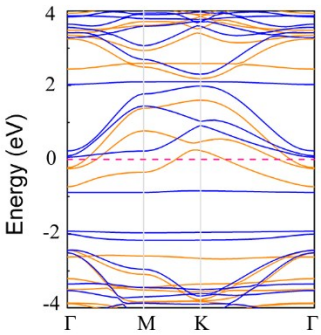


**$Co_1@C_2N$**

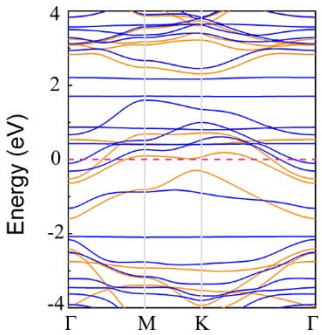


**$Co_2@C_2N$**

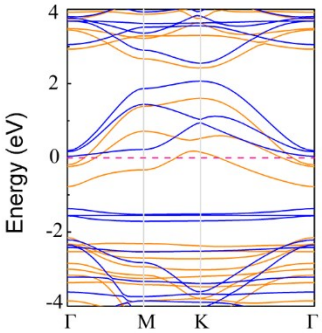


**$Ni_1@C_2N$**

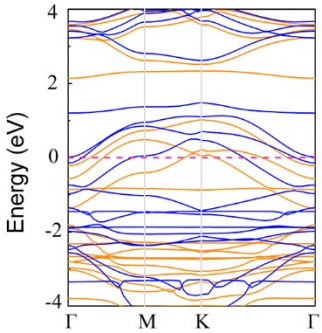


**$Ni_2@C_2N$**

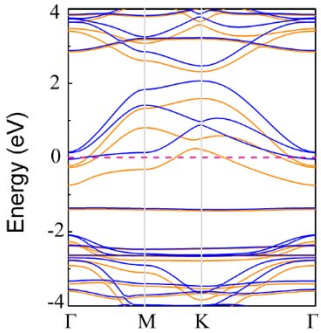


**$Cu_1@C_2N$**

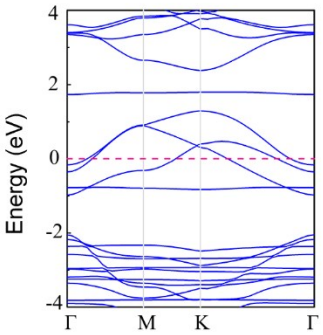


**$Cu_2@C_2N$**

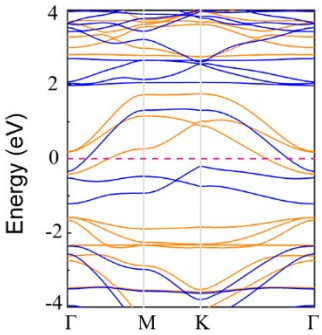


**$Mo_1@C_2N$**

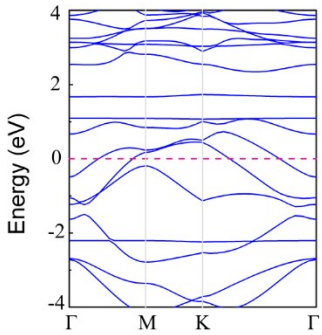


**$Mo_2@C_2N$**

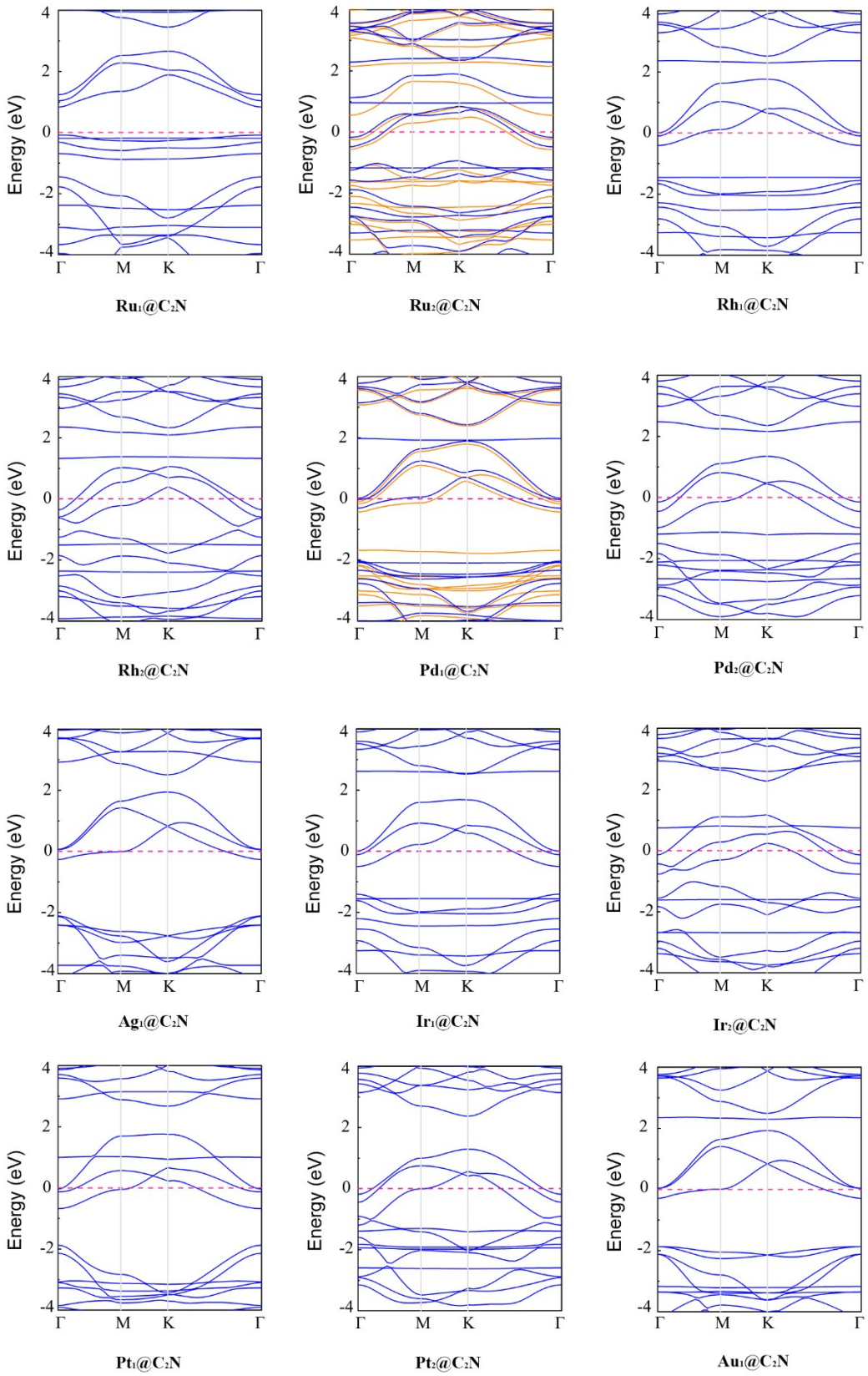


Fig. S3 Band structures of $TM_x@C_2N$ near Fermi level computed at HSE06 level. The Fermi level is set to zero.

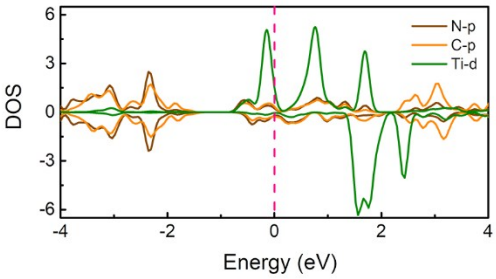


**$Ti_1@C_2N$**

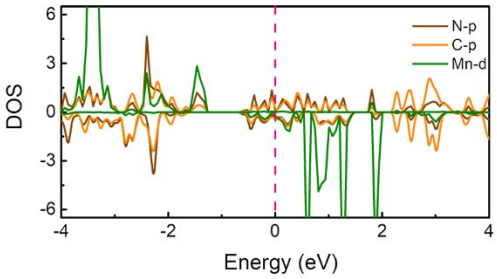


**$Mn_1@C_2N$**

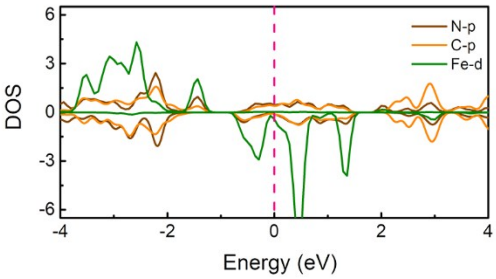


**$Fe_1@C_2N$**

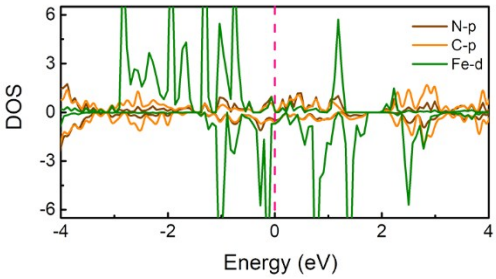


**$Fe_2@C_2N$**

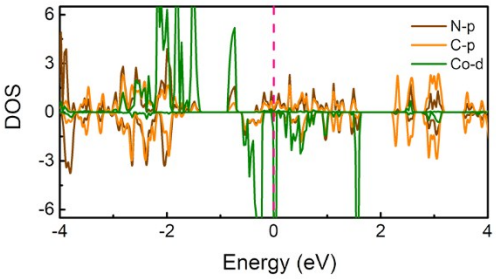


**$Co_1@C_2N$**

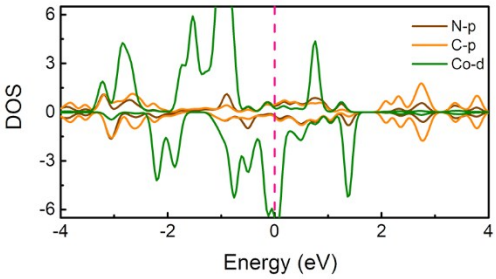


**$Co_2@C_2N$**

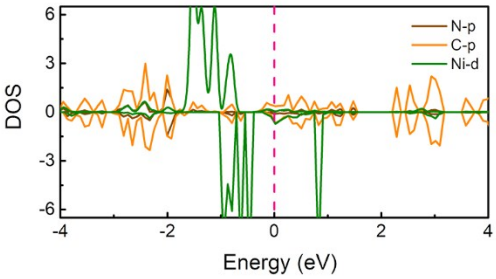


**$Ni_1@C_2N$**

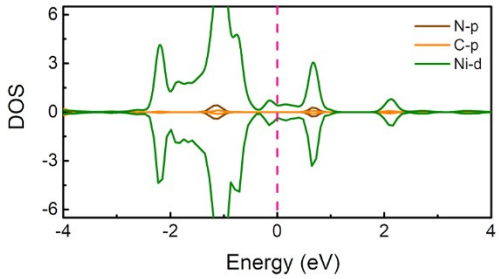


**$Ni_2@C_2N$**

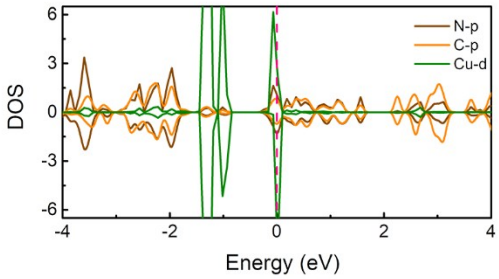


**$Cu_1@C_2N$**

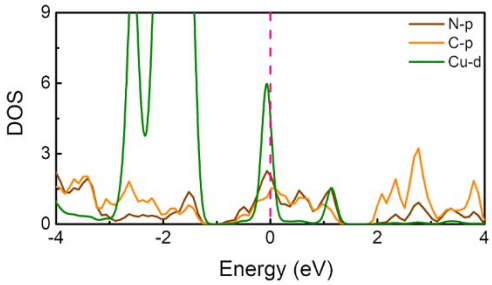


**$Cu_2@C_2N$**

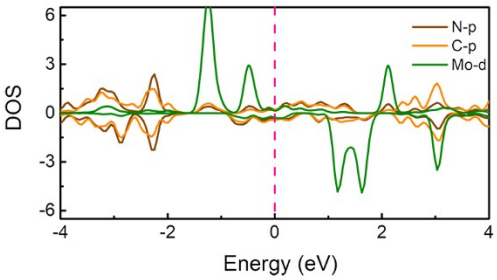


**$Mo_1@C_2N$**

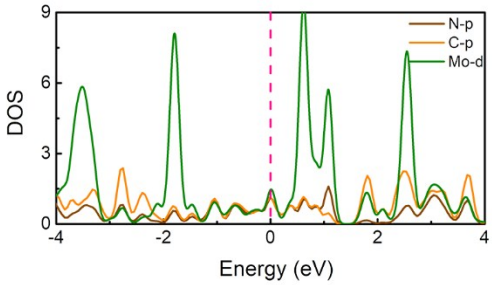


**$Mo_2@C_2N$**

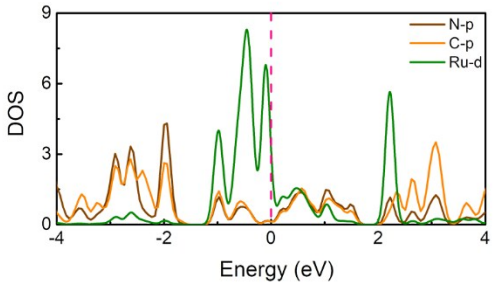


**$Ru_1@C_2N$**

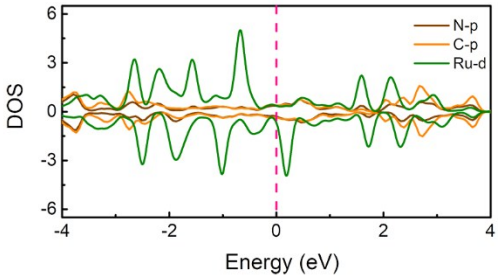


**$Ru_2@C_2N$**

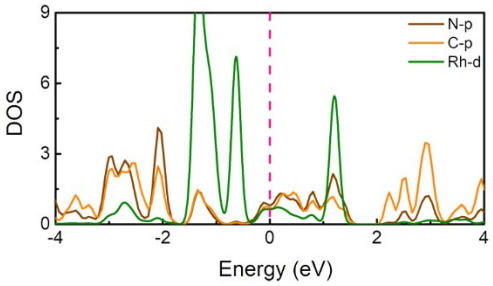


**$Rh_1@C_2N$**

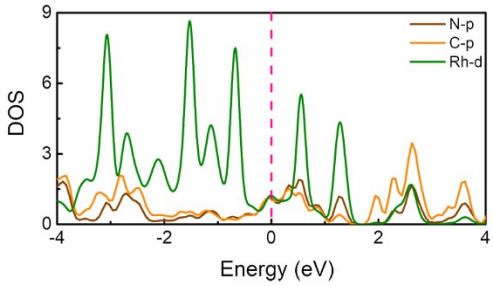


**$Rh_2@C_2N$**

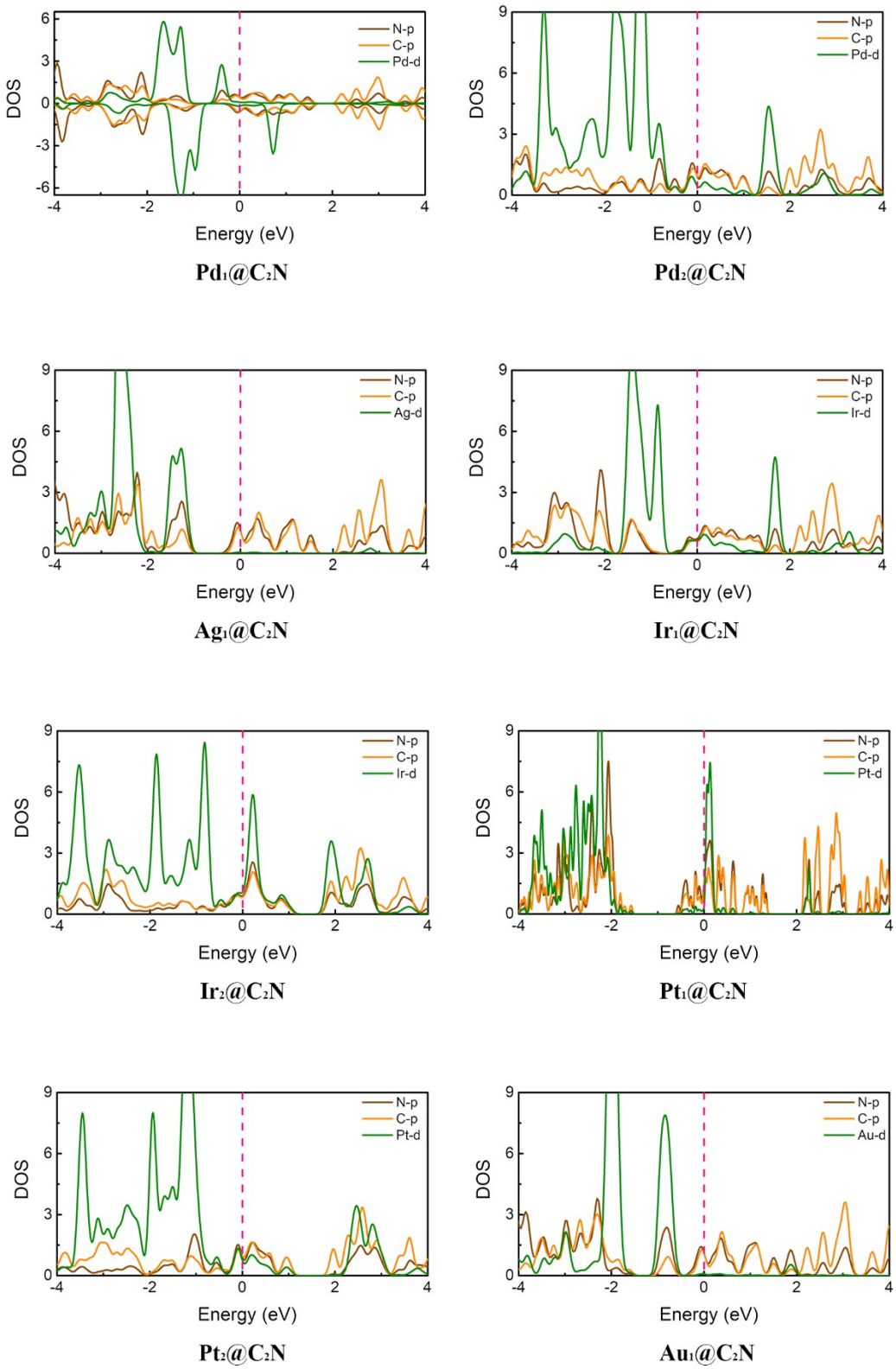


Fig. S4 Computed projected density of states (PDOS) for $TM_x@C_2N$. The Fermi level is set to be zero.

Table S4. Computed Gibbs free energy changes (eV) for hydrogen adsorption on TM ($\Delta G_H$(TM)) and N ($\Delta G_H$(N)) atoms. The promising candidates ($|\Delta G_H| < 0.2$ eV) are highlighted in red typeface. – represents that after the structural optimization, the adsorbed H atoms move to the TM sites.

| $TM_x@C_2N$ | $\Delta G_H$ (TM) | $\Delta G_H$ (N) | $TM_x@C_2N$ | $\Delta G_H$ (TM) | $\Delta G_H$ (N) |
|---|---|---|---|---|---|
| $Ti_1@C_2N$ | -0.05 | 0.05 | $Mn_1@C_2N$ | 0.57 | -0.15 |
| $Fe_1@C_2N$ | 0.45 | – | $Fe_2@C_2N$ | -0.71 | 0.74 |
| $Co_1@C_2N$ | 0.50 | -0.60 | $Co_2@C_2N$ | -0.67 | -0.19 |
| $Ni_1@C_2N$ | 0.62 | -0.54 | $Ni_2@C_2N$ | -0.05 | 0.58 |
| $Cu_1@C_2N$ | 0.75 | -0.56 | $Cu_2@C_2N$ | -0.86 | 0.03 |
| $Mo_1@C_2N$ | -0.02 | – | $Mo_2@C_2N$ | -0.79 | 0.81 |
| $Ru_1@C_2N$ | -0.44 | – | $Ru_2@C_2N$ | -0.09 | 0.48 |
| $Rh_1@C_2N$ | 0.31 | 1.14 | $Rh_2@C_2N$ | -0.82 | 0.22 |
| $Pd_1@C_2N$ | 0.98 | -0.49 | $Pd_2@C_2N$ | -0.37 | – |
| $Ag_1@C_2N$ | 1.51 | -0.22 | $Ir_1@C_2N$ | -0.09 | 1.29 |
| $Ir_2@C_2N$ | -1.21 | 0.25 | $Pt_1@C_2N$ | -0.35 | -0.64 |
| $Pt_2@C_2N$ | -0.81 | 0.72 | $Au_1@C_2N$ | 0.32 | -0.43 |

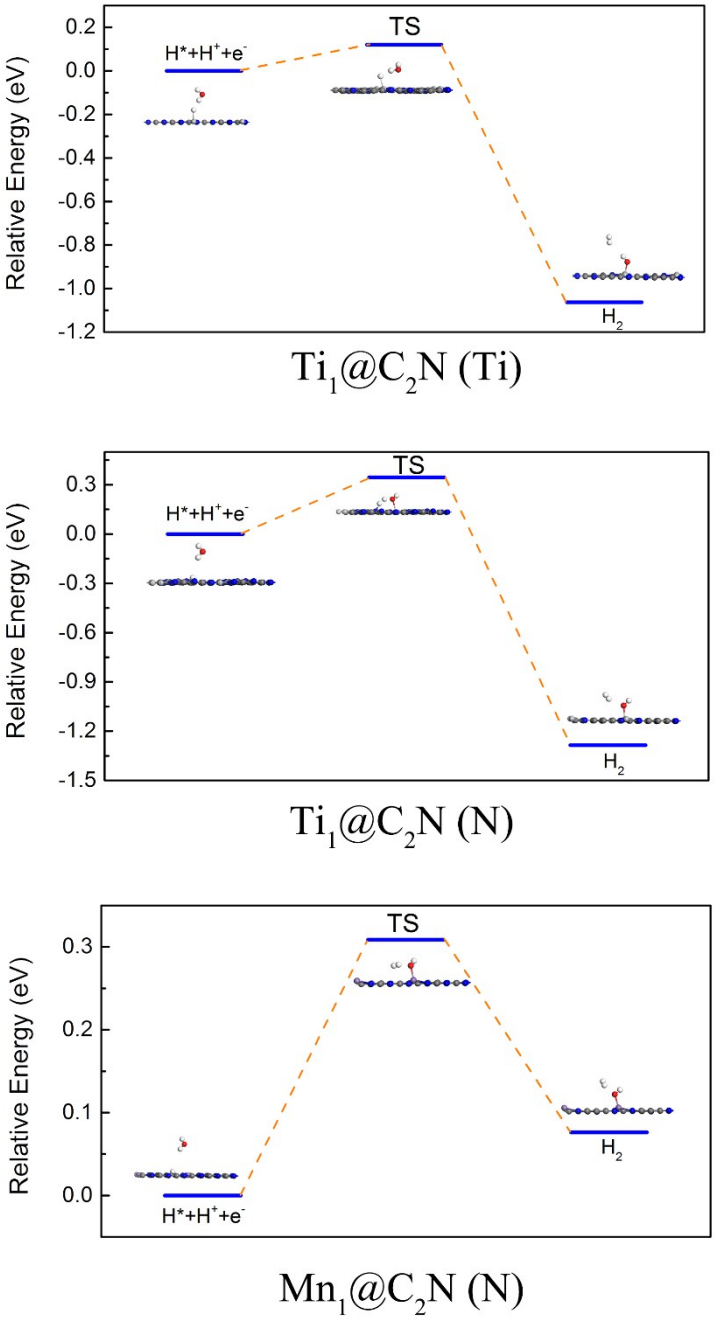


Fig. S5 HER on $Ti_1@C_2N$ and $Mn_1@C_2N$ catalysts.

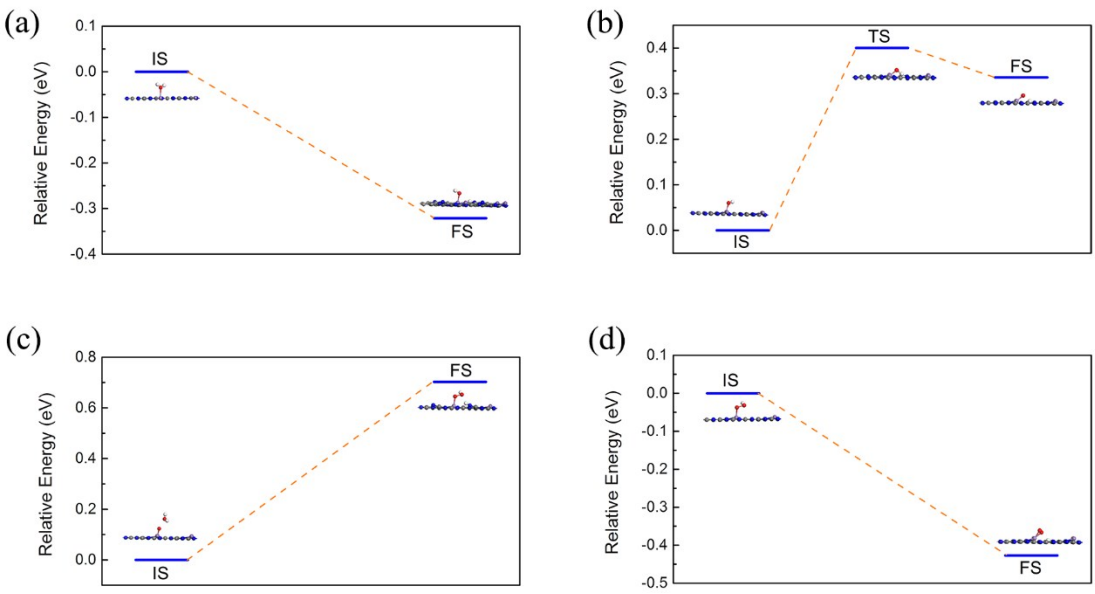


Fig. S6 OER on $Mn_1@C_2N$ catalyst.

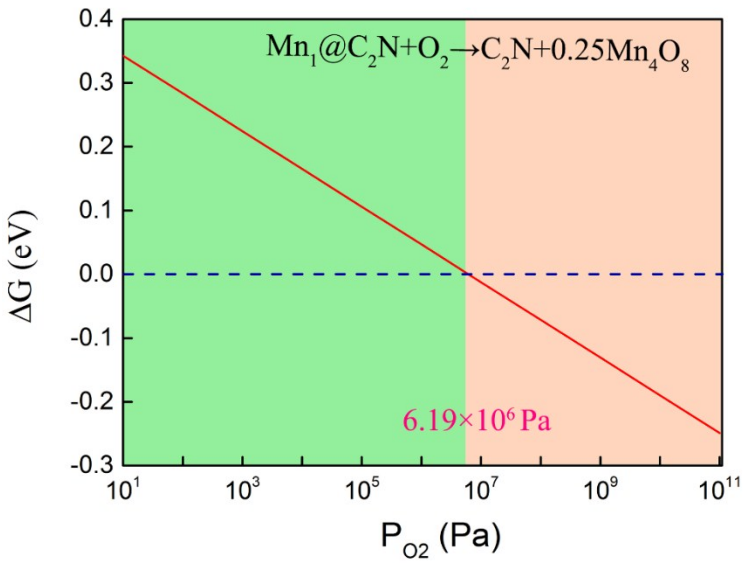


Fig. S7 Gibbs free energy change (ΔG) of Mn oxidation ($Mn_1@C_2N + O_2 \rightarrow C_2N + \frac{1}{4}Mn_4O_8$) as the function of $O_2$ partial pressure ($P_{O_2}$) at 298.15 K. The green and orange regions mean the formation of $Mn_1@C_2N$ and Mn-$O_2$ clusters, respectively.

The chemical potential of $O_2$ was computed based on:

$$\mu_{O_2} = H^o(T) - H^o(0) - TS^o(T) + k_B T \ln\left(\frac{P}{P^o}\right)$$

where $H^o$ and $S^o$ are the enthalpy and entropy at the pressure $P^o$ = 1 bar, respectively. T = 298.15 K was used.

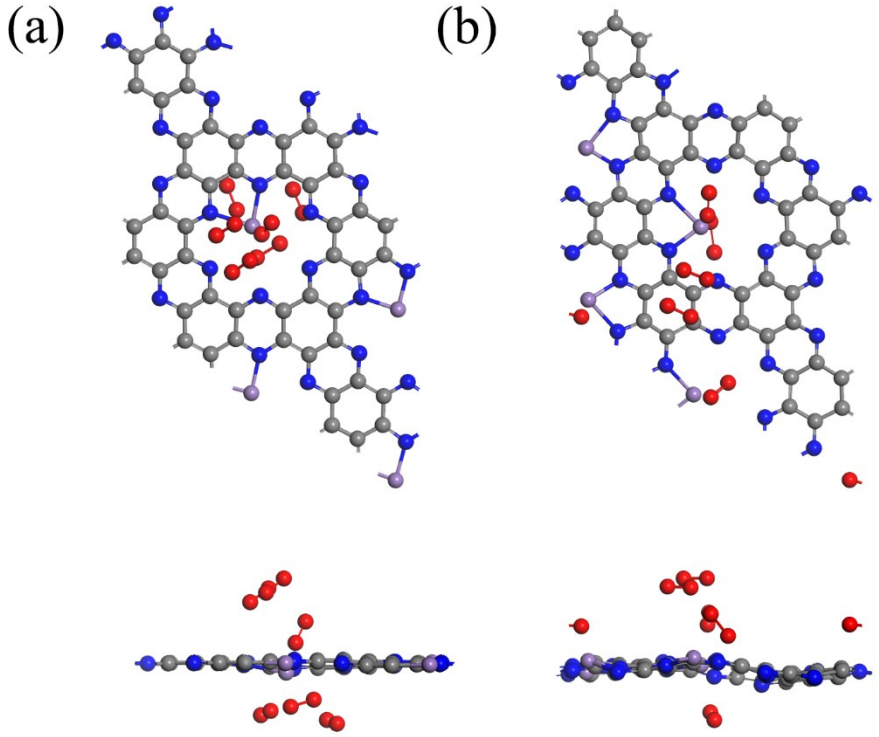


Fig. S8 (a) Top (upper) and side (lower) view of atomic structures of six oxygen molecules around the Mn atom of $Mn_1@C_2N$. (b) Snapshots of the equilibrium structure at 500 K after 10 ps AIMD simulations.